Supporting Information for

J-Aggregation induced emission enhancement of BODIPY dyes via H-bonding directed supramolecular polymerization：The importance of substituents at boron

Yongjie Zhang,†[a] Siyuan Yuan,†[a] Ping Liu,[a] Lei Jing,[a] Hongfei Pan,[a] Xiang-Kui Ren*[a,b] and Zhijian Chen*[a,b]

[a.] School of Chemical Engineering and Technology, Tianjin University, Tianjin, 300072 (China) E-mail: zjchen@tju.edu.cn; renxiangkui@tju.edu.cn.

[b.] Collaborative Innovation Center of Chemical Science and Chemical Engineering (Tianjin), Tianjin University, Tianjin, 300072 (China).

† These authors contributed equally to this work.

DOI: 10.1002/anie.2017XXXXX

Table of Contents

1. General Methods 2
2. Synthesis and characterization 3
3. UV/Vis absorption spectroscopic studies 13
5. Temperature-dependent and time-resolved fluorescence spectroscopic studies 15
6. Studies based on cooperative supramolecular polymerization model 19
7. Concentration-dependent ^{1}H NMR spectroscopic studies 21
8. Studies based on molecular exciton theory 23
9. References 24

1. General Methods

Chemicals and reagents: Solvents and reagents in synthesis process were purchased from commercial suppliers and used without further purification, unless otherwise noted. Products were purified by column chromatography with silica gel (300-400 mesh).

NMR spectroscopy: ^{1}H and ^{13}C NMR spectra of the compounds were recorded on Bruker AVANCE III HD (400 MHz) spectrometer using tetramethylsilane (TMS) as internal standard. Multiplicities for proton signals are abbreviated as *s*, *d*, *t*, and *m* for singlet, doublet, triplet, and multiplet, respectively.

Mass spectrometry: Mass spectra were measured on a Bruker Daltonics micrOTOF-QII LC-MS system.

UV/Vis absorption spectroscopy: UV/Vis absorption spectra were recorded on an Agilent Technologies Cary 300 UV/Vis spectrophotometer equipped with a SPV 1 × 1 temperature controller. The solvents for spectroscopic studies were spectroscopic grade and used as received. The spectra were recorded in quartz glass cuvettes and the molar extinction coefficients ε was calculated according to Lambert-Beer's law: $A = \varepsilon bc$.

Fluorescence spectroscopy: Steady-state and time-resolved fluorescence spectroscopic studies were carried out on an Edinburgh FLS980 spectrofluorometer. All the fluorescence spectra were corrected. The fluorescence quantum yields were determined by FLUOROMAX-4 fluorescence spectrometer with an integrating sphere (from Fluorolog,Horiba JobinYvon).

Atomic force microscopy: AFM measurements were performed under ambient conditions using a Bruker Dimension icon system operating in tapping mode. Silicon cantilevers with a resonance frequency of ~300 kHz were used. Solution of dyes **1a, b** in MCH was drop-casted on mica surface and the solvent was evaporated in air.

2. Synthesis and characterization

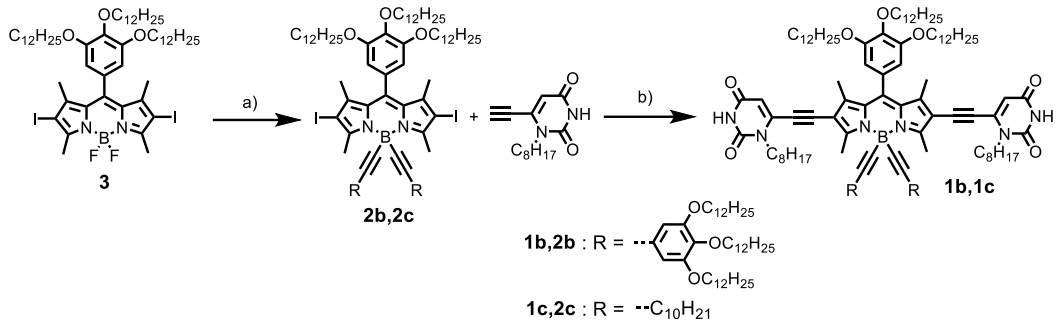

Scheme 1 Reagents and Conditions: a) 3,4,5-tridodecyloxyphenylacetylene (1-dodecyne), C_2H_5BrMg, THF, 60 °C, 6h; b) 6-ethynyl-1-*n*-octyluracil, $Pd(PPh_3)_4$, CuI, TEA, 70°C, 4h.

General procedure for the synthesis of 2b, c

The compound **3**[1] and 6-ethynyl-1-*n*-octyluracil[2] were prepared following our previous reports. C_2H_5BrMg (1 M, THF solution, 1.5 ml) and 3, 4, 5-tri(dodecyloxy)phenylacetylene / 1-dodecyne (1.52 mmol) were subsequently added dropwise to anhydrous THF (5 ml), and the resulting solution was stirred under N_2 at 55 °C to prepare the Grignard reagent. After 2 h, compound **3** (214 mg, 0.19 mmol) was dissolved in anhydrous THF (5 ml) and stirred under N_2 at 60°C, to which the Grignard reagent was added with syringe. The reaction system was stirred under N_2 for another 0.5 h, and monitored by TLC analysis. After completion of the reaction, the resulting mixture was cooled to the room temperature. The solvent was removed in vacuum after which the residue was re-dissolved in CH_2Cl_2 (100 mL) and washed with water (100 mL × 3) and then dried over Na_2SO_4. The solvent was evaporated in vacuum and purification of the crude product by column chromatography with CH_2Cl_2/ petroleum ether (1:2, v/v) and evaporation of the solvent gave the target compound as an orange powder.

Compound 2b Yield: 75%. ^{1}H NMR(400MHz, Chloroform-d) δ 6.60 (*s*, 4H), 6.48 (*s*, 2H), 4.04 (*t*, *J* = 6.4 Hz, 2H), 3.98 – 3.88 (*m*, 16H), 2.96 (*s*, 6H), 1.83 – 1.75 (*m*, 14H), 1.74 – 1.67 (*m*, 6H), 1.58 (*s*, 6H), 1.46 (*t*, *J* = 10.8 Hz, 20H), 1.27 (*d*, *J* = 9.7 Hz, 140H), 0.91 – 0.85 (*m*, 27H). ^{13}C NMR (100 MHz, $CDCl_3$, ppm): δ = 156.22, 154.34, 152.86, 143.40, 141.38, 138.90, 138.62, 129.88, 129.55, 119.39, 110.39, 106.35, 95.87, 85.92, 77.16, 73.79, 73.50, 69.48, 69.22, 31.96, 30.33, 29.78, 29.74, 29.72, 29.68, 29.63, 29.45, 29.39, 29.34, 26.14, 26.04, 22.72, 17.75, 17.14, 14.13.

Compound 2c Yield: 89%. ^{1}H NMR (400 MHz, Chloroform-d): δ = 6.45 (*s*, 2H), 4.02 (*t*, *J* = 8 Hz, 2H), 3.89 (*t*, *J* = 4 Hz, 4H), 2.84 (*s*, 6H), 2.20-2.16 (*m*, 6H), 2.15-2.13 (*m*, 2H), 1.94-1.93 (*t*, *J* = 4 Hz, 6H), 1.79-1.74 (*m*, 6H), 1.54-1.49 (*m*, 12H), 1.43-1.35 (*m*, 6H), 1.28-1.26 (*m*, 66H), 0.88 (*t*, *J* = 8 Hz, 15H). ^{13}C NMR (100 MHz, $CDCl_3$, ppm): δ = 155.89, 154.22, 142.83, 141.06, 138.76, 130.10, 129.34, 106.44, 96.08, 85.74, 84.70, 73.72, 69.42, 68.04, 31.96, 31.93, 29.78, 29.72, 29.68, 29.64, 29.60, 29.40, 29.34, 29.26, 29.14, 26.16, 26.04, 22.73, 19.85, 18.42, 17.52, 17.05, 14.12.

General procedure for the synthesis of 1b, c

A mixture of compound **2b, c** (0.133 mmol), $Pd(PPh_3)_4$ (23 mg, 0.02 mmol), CuI (3.8 mg, 0.02 mmol), 6-ethynyl-1-octyluracil (82.5 mg, 2.5 mmol) and trimethylamine (10 mL) was stirred under N_2 at 70 °C for 4 h and the reaction progress was monitored by TLC analysis. After completion, the reaction was cooled to room temperature and water was added (10 ml). The resulting mixture was extracted with CH_2Cl_2 (20 ml × 3) and the organic layer was dried over Na_2SO_4. The volatiles were removed in vacuum, and the residue was purified by column chromatography with CH_2Cl_2 / Methanol (40 : 1, v / v). Evaporation of the solvent gave the target compounds as red powder.

BODIPY dye 1b. Yield: 37.6%. m.p. 227–230 °C. ^{1}H NMR (400 MHz, $CDCl_3$) δ 8.14 (*s*, 2H), 6.60 (*s*, 4H), 6.50 (*s*, 2H), 5.92 (*s*, 2H), 4.08 – 3.97 (*m*, 6H), 3.93 (*t*, *J* = 6.2 Hz, 16H), 2.99 (*s*, 6H), 1.79 (d, *J* = 6.6 Hz, 6H), 1.70 (*s*, 14H), 1.57 (*s*,

16H), 1.45 (*s*, 20H), 1.26 (*s*, 154H), 0.91 – 0.82 (*m*, 33H). ^{13}C NMR (101 MHz, $CDCl_3$) *δ* 162.08, 159.40, 154.65, 152.99, 150.51, 145.08, 139.05, 138.85, 130.25, 118.83, 113.92, 110.46, 106.05, 94.49, 88.02, 73.56, 69.72, 69.32, 46.70, 31.94, 31.92, 31.66, 30.33, 29.75, 29.70, 29.65, 29.61, 29.48, 29.45, 29.43, 29.38, 29.36, 29.19, 29.05, 28.89, 26.57, 26.16, 26.13, 26.06, 22.68, 22.54, 15.50, 14.10, 14.03, 13.74. HRMS (MALDI-TOF): calculated for $C_{171}H_{281}BF_2N_6O_{13}$ $[M+H]^+$ 2640.9 m/z, found 2640.2 m/z. Elemental analysis: calculated for $C_{171}H_{281}BF_2N_6O_{13}$: C 77.80%, H 10.73%, N 3.18%; found: C 77.69%, H 10.59%, N 3.09%.

BODIPY dye 1c. Yield: 58%. m.p. 222–225 °C. ^{1}H NMR (400 MHz, $CDCl_3$) *δ* 8.31 (*s*, 2H), 6.46 (*s*, 2H), 5.91 (*d*, *J* = 2.2 Hz, 2H), 4.01 (*dd*, *J* = 13.7, 6.9 Hz, 6H), 3.90 (*t*, *J* = 6.5 Hz, 4H), 2.89 (*s*, 6H), 2.17 (*t*, *J* = 7.3 Hz, 4H), 1.79 (*q*, *J* = 7.9 Hz, 6H), 1.73 (*s*, 4H), 1.66 (*s*, 6H), 1.60 (*s*, 4H), 1.54 – 1.48 (*m*, 6H), 1.44 (*d*, *J* = 7.8 Hz, 6H), 1.25 (*s*, 90H), 0.89 – 0.85 (*m*, 21H). ^{13}C NMR (101 MHz, $CDCl_3$) δ 162.03, 159.12, 154.54, 150.49, 144.76, 139.31, 138.97, 130.11, 113.67, 106.01, 105.87, 97.20, 94.89, 87.88, 73.88, 69.67, 46.73, 31.94, 31.91, 31.72, 30.34, 29.76, 29.69, 29.64, 29.61, 29.42, 29.39, 29.35, 29.26, 29.22, 29.18, 29.13, 28.92, 26.65, 26.16, 26.05, 22.68, 22.58, 19.78, 15.27, 14.09, 14.05, 13.67. HRMS (ESI): calculated for $C_{107}H_{169}BF_2N_6O_7$ $[M + H]^+$ 1663.3 m/z, found 1663.7 m/z. Elemental analysis: calculated for $C_{107}H_{169}BF_2N_6O_7$: C 77.31%, H 10.25%, N 5.06%; found: C 77.13%, H 10.15%, N 4.99%.

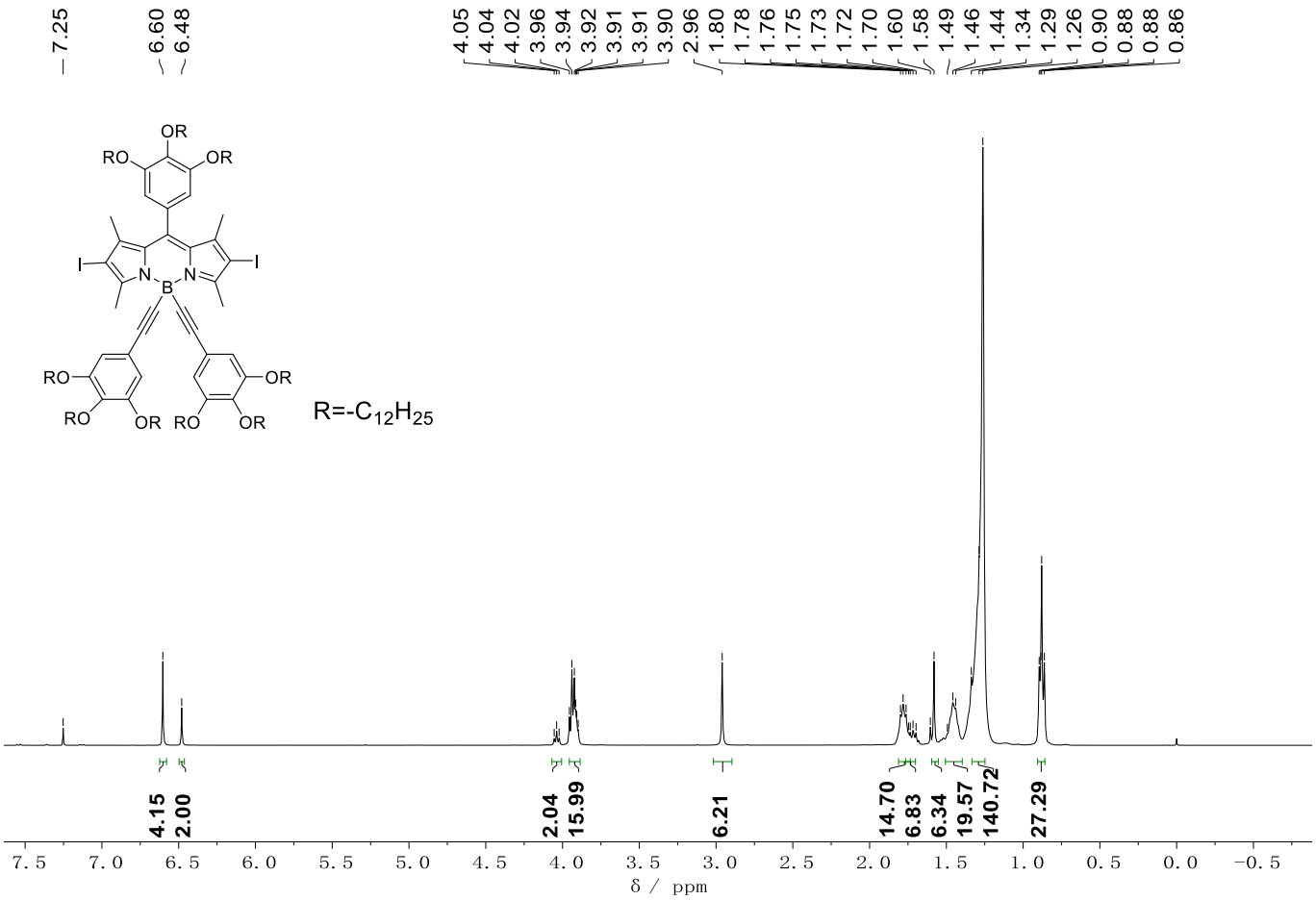

Fig. S1 The ^{1}H NMR spectrum (400 MHz) with chemical molecular structure of compound **2b** in $CDCl_3$ at 293 K.

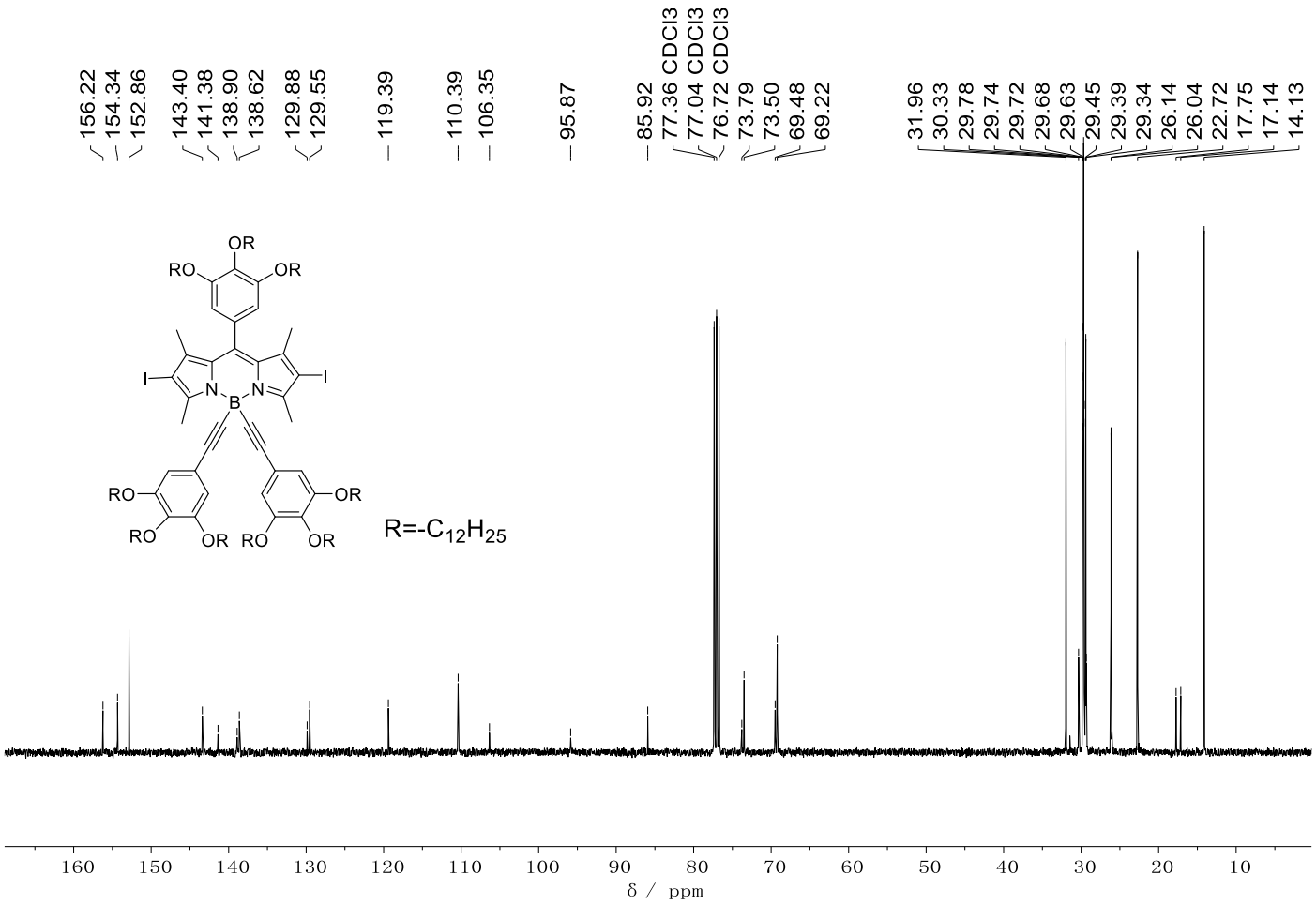

Fig. S2 The ^{13}C NMR spectrum (101 MHz) with chemical molecular structure of compound **2b** in $CDCl_3$ at 293 K.

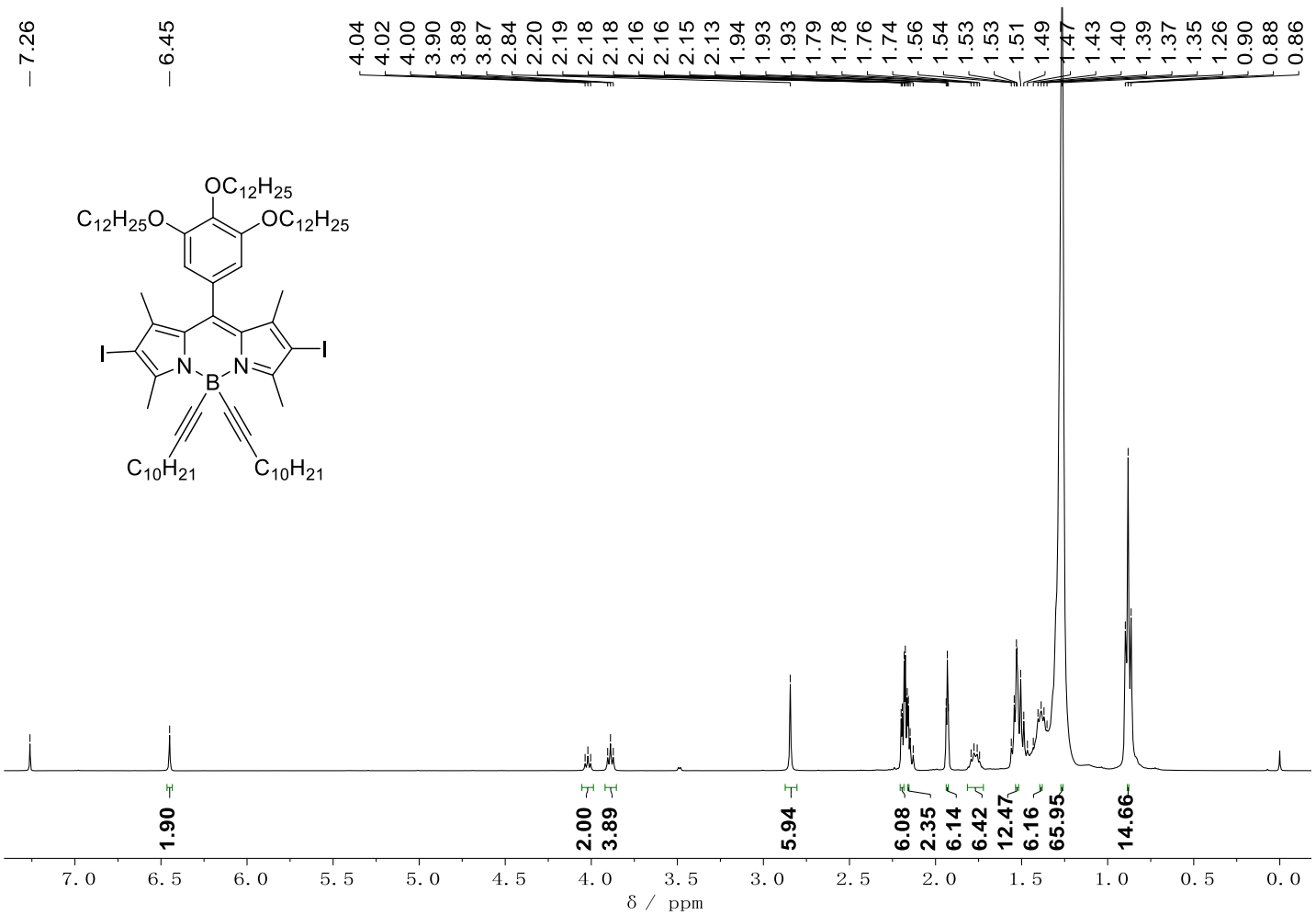

Fig. S3 The ^{1}H NMR spectrum (400 MHz) with chemical molecular structure of compound **2c** in $CDCl_3$ at 293 K.

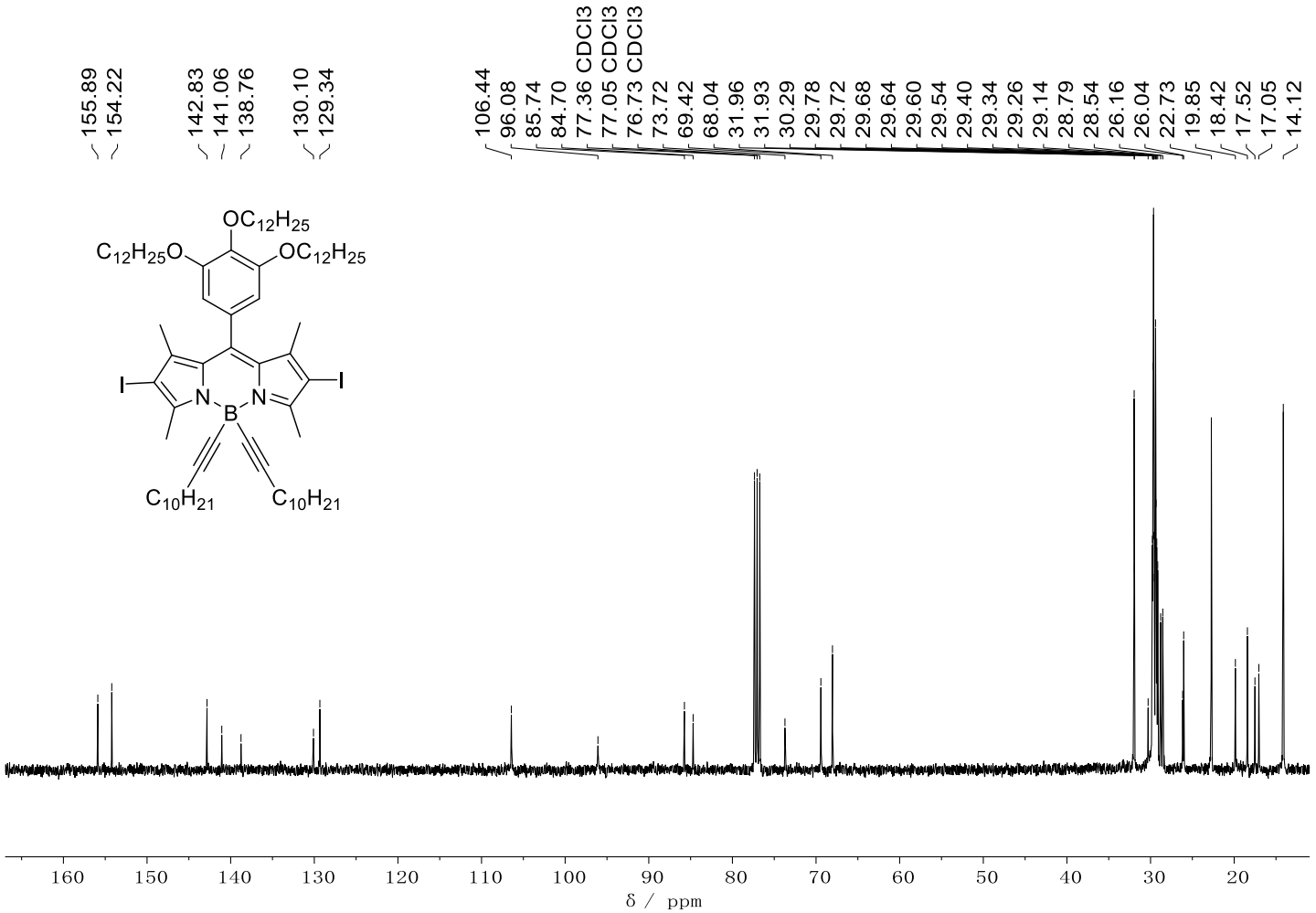

Fig. S4 The ^{13}C NMR spectrum (101 MHz) with chemical molecular structure of compound **2c** in $CDCl_3$ at 293 K

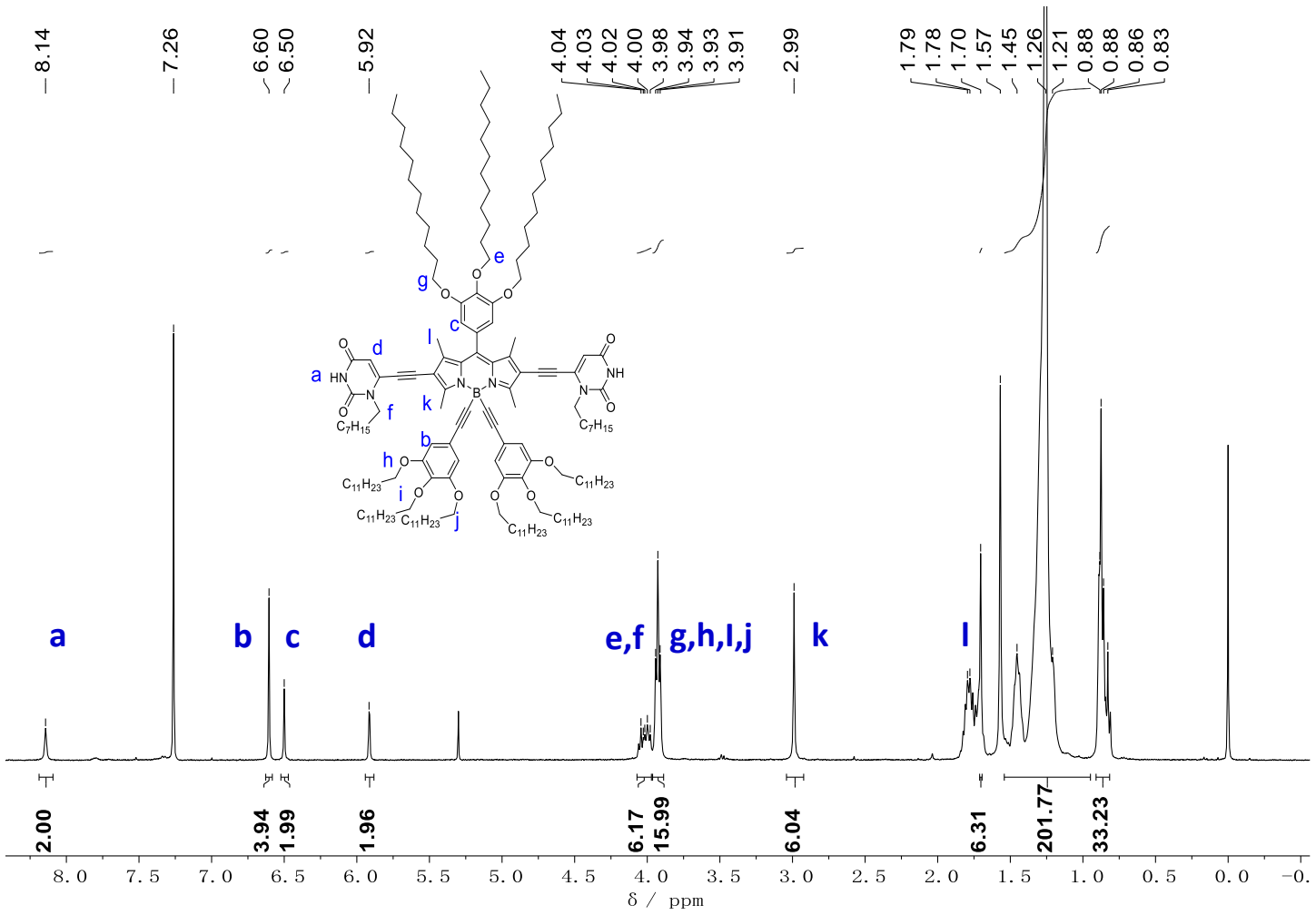

Fig. S5 The ^{1}H NMR spectrum (400 MHz) with chemical molecular structure of compound **1b** in $CDCl_3$ at 293 K.

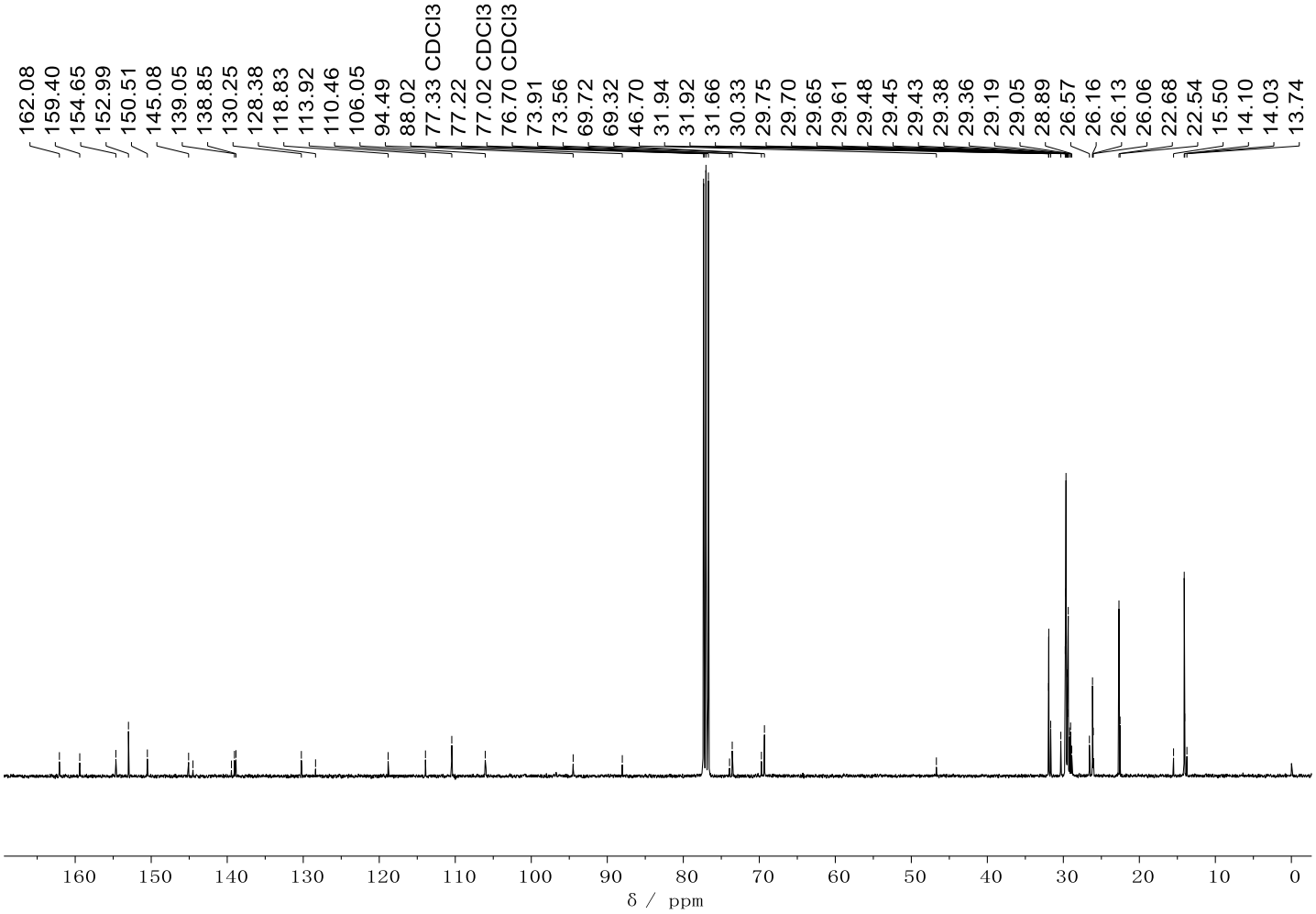

Fig. S6 The ^{13}C NMR spectrum (101 MHz) with chemical molecular structure of compound **1b** in $CDCl_3$ at 293 K.

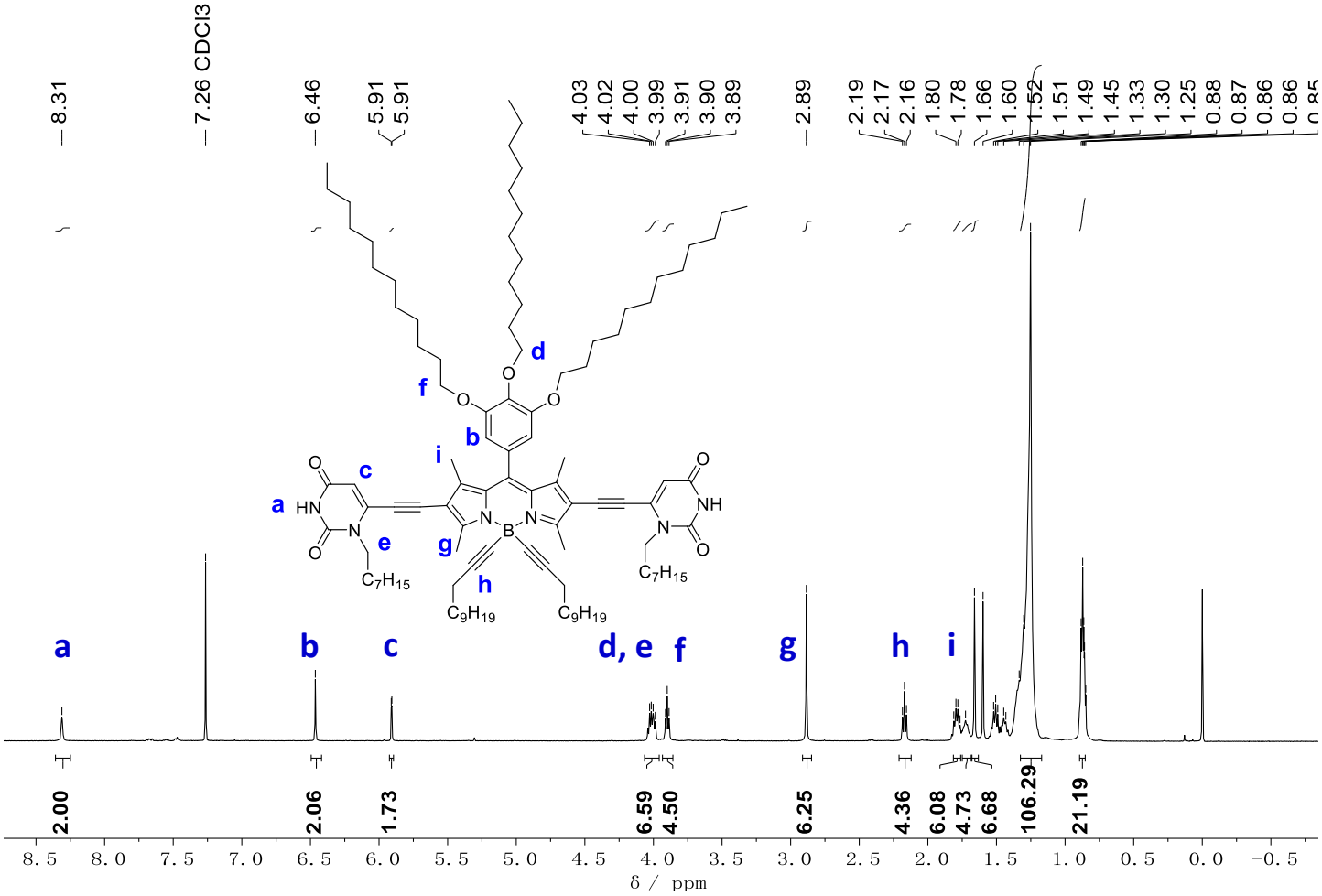

Fig. S7 The ^{1}H NMR spectrum (400 MHz) with chemical molecular structure of compound **1c** in $CDCl_3$ at 293 K.

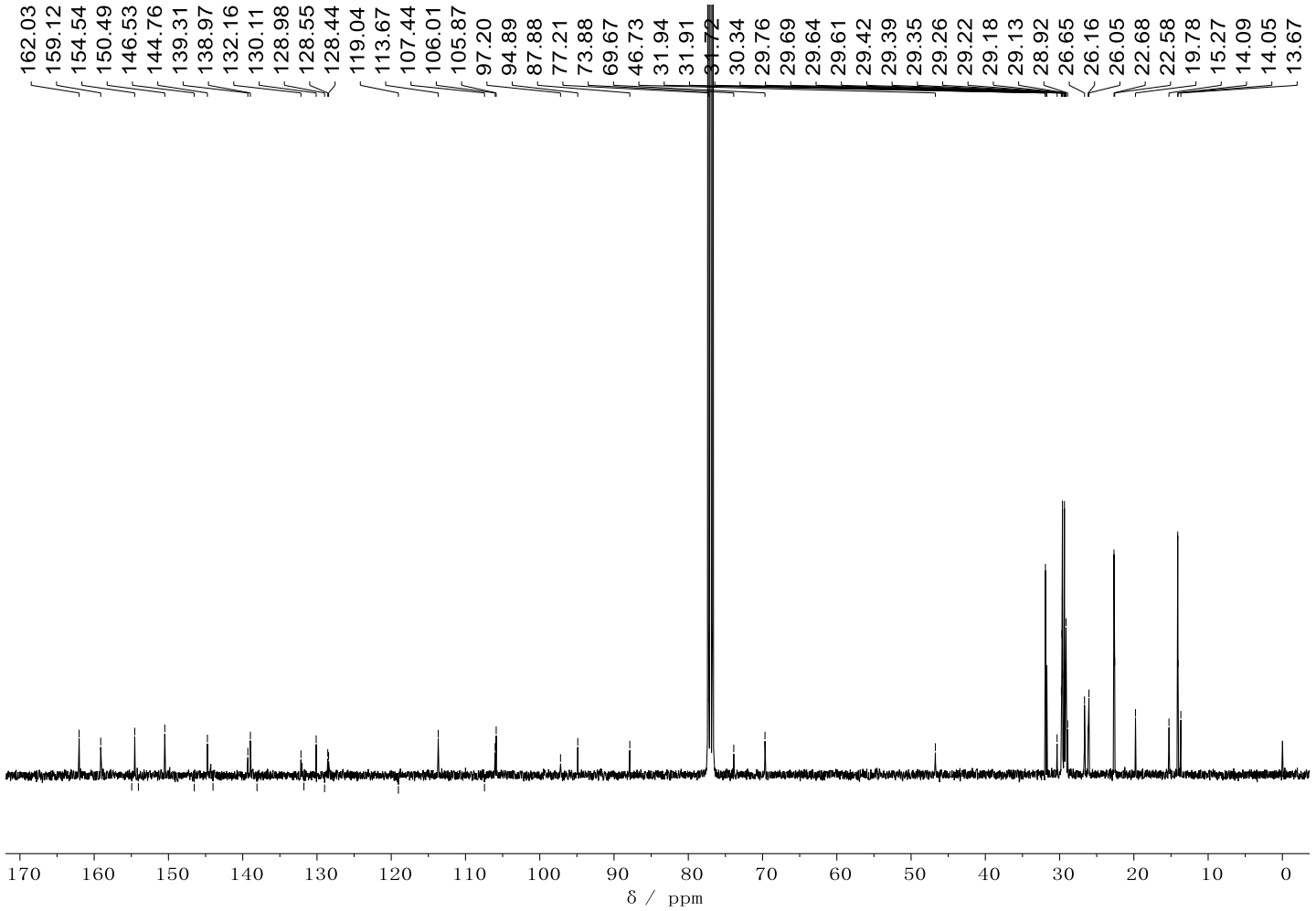

Fig. S8 The ^{13}C NMR spectrum (101 MHz) with chemical molecular structure of compound **1c** in $CDCl_3$ at 293 K.

3. UV/Vis absorption spectroscopic studies

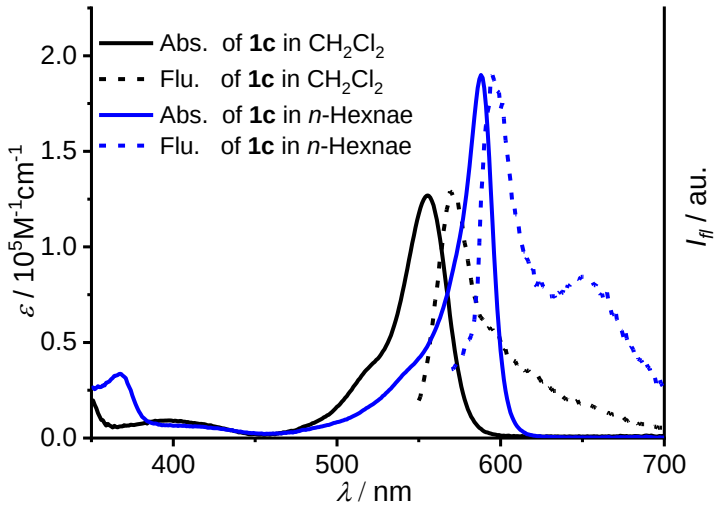

Fig. S9 UV/Vis absorption and fluorescence spectra (λ_{Ex} = 350 nm) of dye **1c** in CH_2Cl_2 ($c_T = 1 \times 10^{-5}$ M, black lines) and *n*-hexane ($c_T = 1 \times 10^{-5}$ M, blue lines).

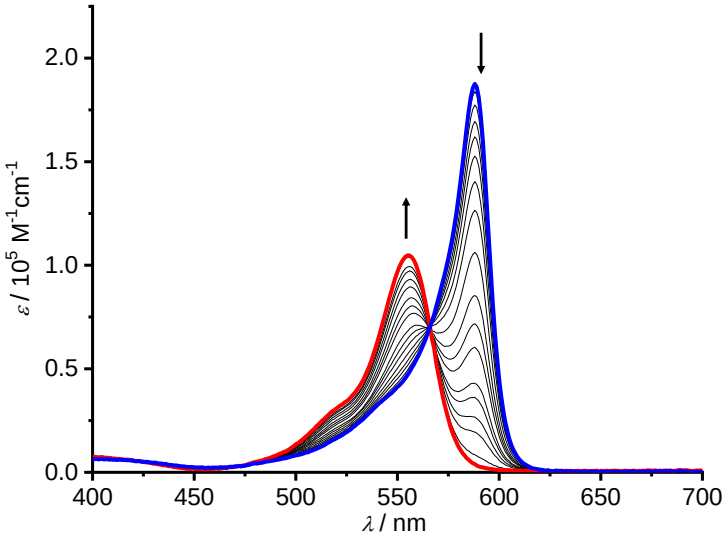

Fig. S10. Temperature-dependent UV/Vis absorption spectra of BODIPY dye **1c** in *n*-hexane ($c_T = 2.0 \times 10^{-6}$ M). The arrows indicate the spectra changing with increasing temperature from 4 to 60°C.

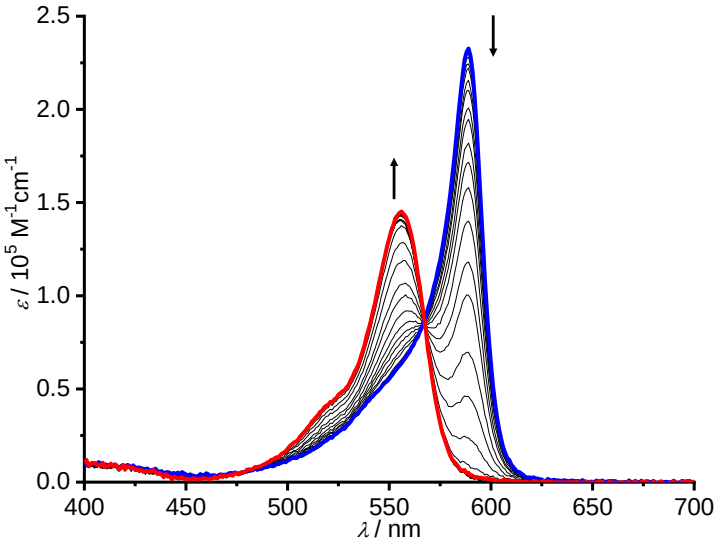

Fig. S11. Temperature-dependent UV/Vis absorption spectra of BODIPY dye **1b** in MCH (c_T = 1.0 × 10^{-5} M). The arrows indicate the spectra changing with increasing temperature from 4 to 68°C.

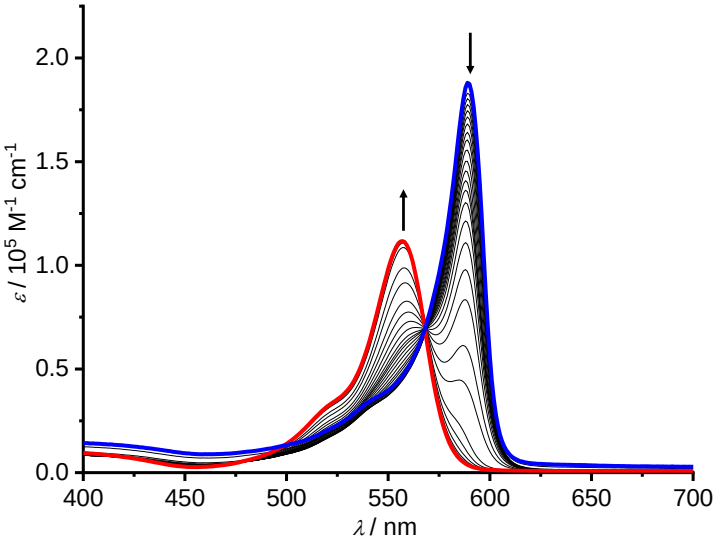

Fig. S12. Temperature-dependent UV/Vis absorption spectra of BODIPY dye **1c** in MCH (c_T = 1.0 × 10^{-5} M). The arrows indicate the spectra changing with increasing temperature from 4 to 68°C.

5. Temperature-dependent and time-resolved fluorescence spectroscopic studies

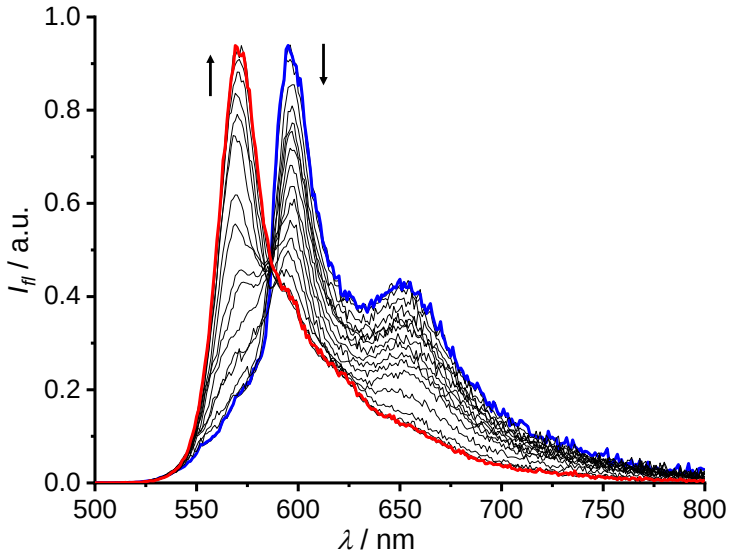

Fig. S13 Temperature-dependent fluorescence spectra of **1c** in *n*-hexane (c_T = 2.0 × 10^{-6} M); Arrows indicate the spectroscopic changes with increasing temperature from 4 to 60 °C.

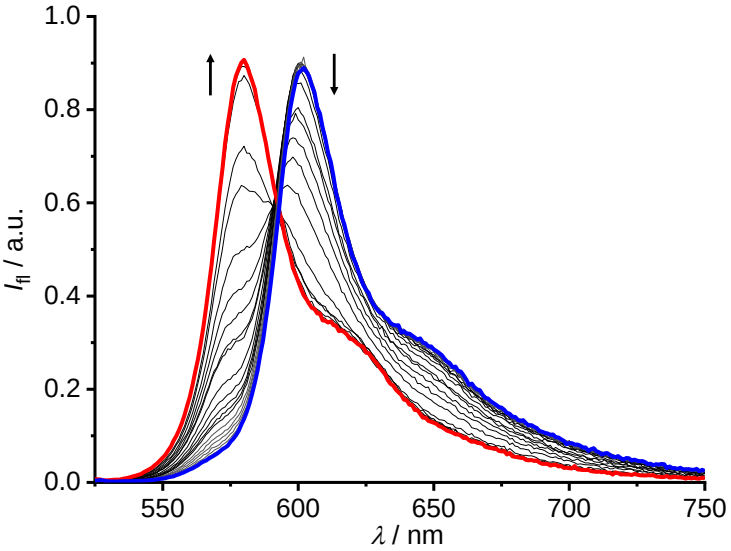

Fig. S14 Temperature-dependent fluorescence spectra of **1b** in MCH (c_T = 5.0 × 10^{-6} M); Arrows indicate the spectroscopic changes with increasing temperature from 4 to 70 °C.

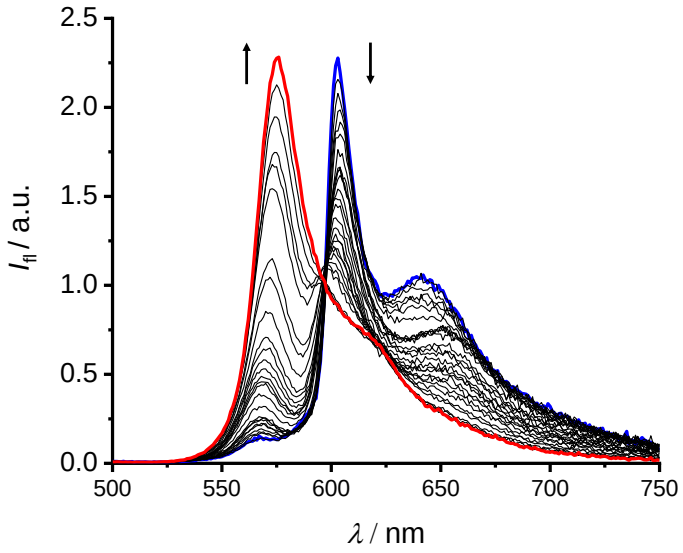

Fig. S15 Temperature-dependent fluorescence spectra of **1c** in MCH (c_T = 5.0 × 10^{-6} M); Arrows indicate the spectroscopic changes with increasing temperature from 4 to 70 °C.

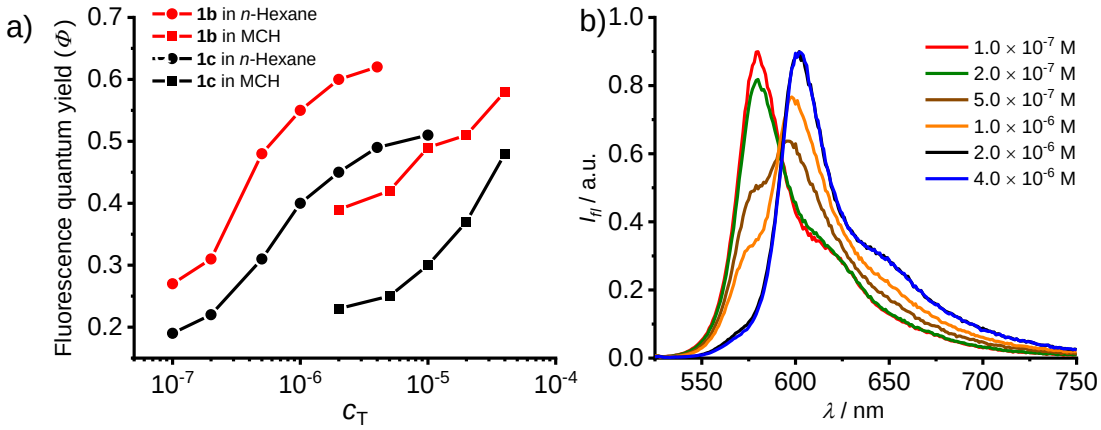

Fig. S16 (a) Concentration-dependent fluorescence quantum yields of dyes **1b, c** in *n*-hexane and MCH at 293 K. (b) Concentration-dependent fluorescence spectra (normalized) of dye **1b** in *n*-hexane.

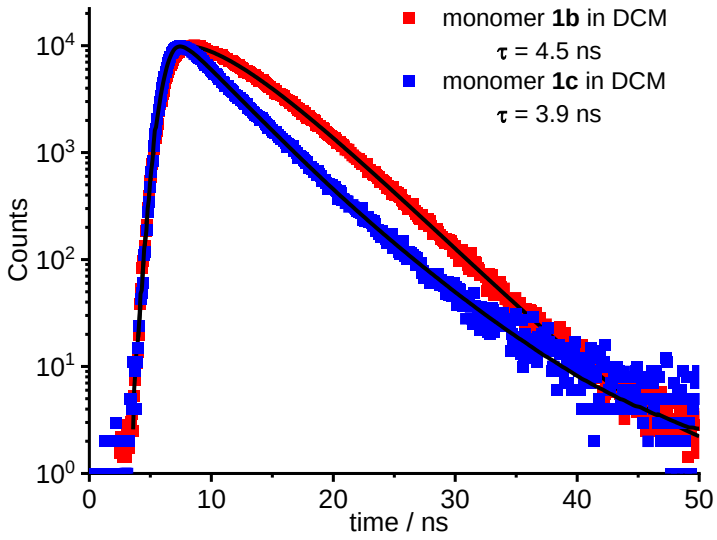

Fig. S17 Time-resolved fluorescence decay for monomers **1b** (c_T = 5.0 × 10^{-5} M, λ_{Ex} = 350 nm, λ_{Em} = 578 nm) and **1c** (c_T = 5.0 ×10^{-5} M, λ_{Ex} = 350 nm, λ_{Em} = 568 nm) in CH_2Cl_2.

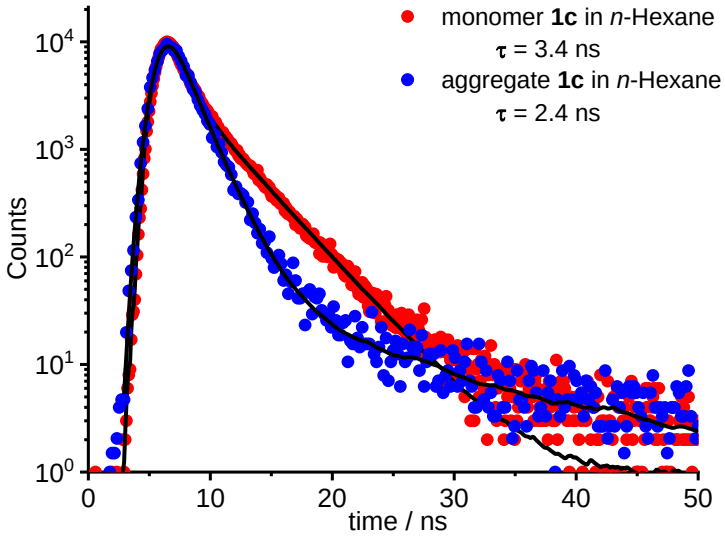

Fig. S18 Time-resolved fluorescence decay for aggregates (c_T = 1.0 × 10^{-5} M, λ_{Ex} = 350 nm, λ_{Em} = 604 nm) and monomers (c_T = 5.0 × 10^{-8} M, λ_{Ex} = 350 nm, λ_{Em} = 570 nm) of **1c** in *n*-hexane.

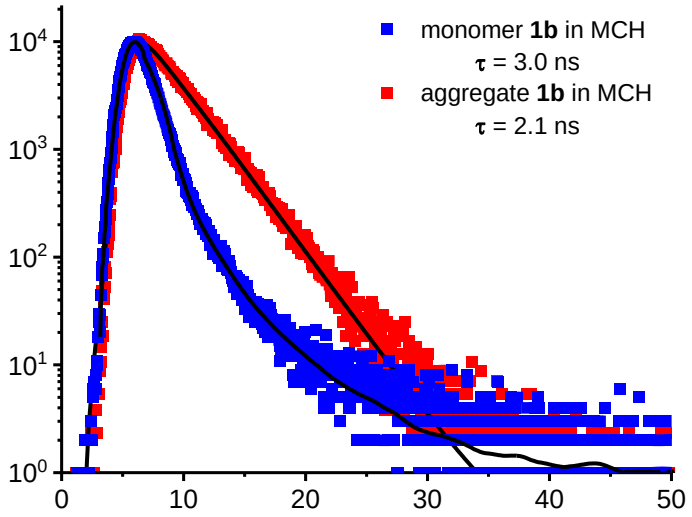

Fig. S19 Time-resolved fluorescence decay for monomers (c_T = 9.0 × 10^{-7} M, λ_{Ex} = 350 nm, λ_{Em} =578 nm) and aggregates (c_T = 5.0 × 10^{-5} M, λ_{Ex} = 350 nm, λ_{Em} = 608 nm) of **1b** in MCH.

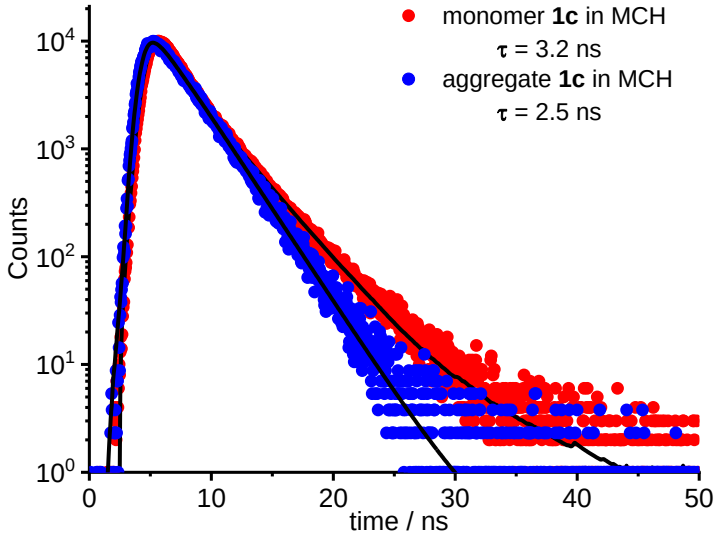

Fig. S20 Time-resolved fluorescence decay for monomer (c_T = 9.0 × 10^{-7} M, λ_{Ex} = 350 nm, λ_{Em} = 570 nm) and aggregates (c_T = 5.0 ×10^{-5}, λ_{Ex} = 350 nm, λ_{Em} = 603 nm) of **1c** in MCH.

Table S1 Photophysical parameters of BODIPY dyes **1b, c** obtained from time-resolved fluorescence spectroscopy.

Dyes	solvent	τ_{mon} / ns	χ^2_{mon}	τ_{1agg} / ns (%)[a]	τ_{2agg} / ns (%)[a]	τ_{agg} / ns [b]	χ^2_{agg}
1b	CH_2Cl_2	3.9	1.13	N/A	N/A	N/A	N/A
1c	CH_2Cl_2	4.5	1.19	N/A	N/A	N/A	N/A
1b	*n*-Hexane	3.7	1.15	0.79 (98%)	4.83 (2%)	0.9	1.15
1c	*n*-Hexane	3.4	0.98	3.35 (56.82%)	1.09 (43.18%)	2.4	1.22
1b	MCH	3.0	0.96	0.89 (52.15%)	3.51 (47.58%)	2.1	1.12
1c	MCH	3.2	1.21	3.45 (58.33%)	1.17 (41.67%)	2.5	1.11

[a] Components of bi-exponential fluorescence lifetimes and pre-exponential factors (in brackets).

[b] Averaged fluorescence lifetimes

6. Studies based on cooperative supramolecular polymerization model

Nucleation-Elongation model

The fraction of aggregated molecules α_{agg} at a certain concentration and temperature can be estimated according to equation 1 based on the assumption that the dye molecules aggregate fully (α_{agg} = 1) at lowest temperature or highest concentration and exist as monomers (α_{agg} = 0) at highest temperature or lowest concentration. The ε_{mon} and ε_{agg} stands for molar absorption coefficients of the monomer and fully aggregated state respectively.

$$\alpha_{agg} = 1 - \frac{\varepsilon - \varepsilon_{agg}}{\varepsilon_{\mathrm{mon}} - \varepsilon_{agg}} \tag{1}$$

For the cooperative model proposed by Meijer et al.,[3] the supramolecular polymerization is composed of a nucleation process at higher temperature range and an elongation process at lower temperature range. Accordingly, in the elongation regime, the fraction of aggregated species (α_{agg}) in temperature-dependent experiments can be described as equation 2:

$$\alpha_{agg} = \alpha_{SAT}\left\{1 - exp\left[\frac{-\Delta H_e}{RT_e^2}(T - T_e)\right]\right\} \tag{2}$$

Here, ΔH_e is the enthalpy corresponding to elongation regime, T is the temperature, T_e is the critical elongation temperature, R is the ideal gas constant and α_{SAT} is a parameter introduced to ensure that $\alpha_{agg}/\alpha_{SAT}$ does not exceed unity. At the temperature above T_e (nucleation regime), the fraction of aggregated molecules can be described as equation 3, in which K_a is the dimensionless equilibrium constant of the activation.

$$\alpha_{agg} = K_a^{1/3} exp\left[\left(2/3K_a^{-1/3} - 1\right)\frac{\Delta H_e}{RT_e^2}(T - T_e)\right] \tag{3}$$

The average length of the stack N_n at the T_e is given by equation 4.

$$\langle N_n(T_e)\rangle = \frac{1}{K_a^{1/3}} \tag{4}$$

Goldstein-Stryer model

Concentration-dependent UV/Vis spectroscopic data were analyzed according to the Goldstein-Stryer model.[4] In this model, a nucleus of size s is formed in the nucleation regime through an isodesmic process with an equilibrium constant of K_s while further steps of adding more molecules to the nucleus take place with equal equilibrium constant K ($K > K_s$), i.e. $K_1 = K_2 = ... = K_s$ and $K_{s+1} = K_{s+2} = ... = K$. The cooperativity is reflected by the parameter σ defined as $\sigma = K_s / K$. The relation between dimensionless concentrations Kc_T and Kc_1 can be described as the equation 5, where c_1 is the concentration of the monomer species and c_T is the total concentration of the molecules：

$$Kc_T = \sum_{n=1}^{s} n\sigma^{n-1}(Kc_1)^n + \sum_{n=s+1}^{\infty} n\sigma^{s-1}(Kc_1)^n = \frac{s(Kc_1)^s\sigma^{s-1}}{1-Kc_1} + \frac{(Kc_1)^{s+1}\sigma^{s-1}}{(1-Kc_1)^2} + \frac{K_{c_1}(s(\sigma Kc_1)^{s-1}-1)}{\sigma Kc_1 - 1} -$$

$$\frac{\sigma(Kc_1)^2((\sigma Kc_1)^{s-1}-1)}{(\sigma Kc_1-1)^2} \tag{5}$$

In the meantime, α_{agg} can be calculated from equation 6:

$$\alpha_{agg} = 1 - \alpha_{mon} = 1 - \frac{Kc_1}{Kc_T} \tag{6}$$

Both α_{agg} and Kc_T can be obtained from the data of Kc_1 and the curve of α_{agg} against Kc_T can be drawn. The experiment data extracted from concentration-dependent UV/Vis spectra were collected and manually fitted into the curve for the best match, the results are presented in the main manuscript.

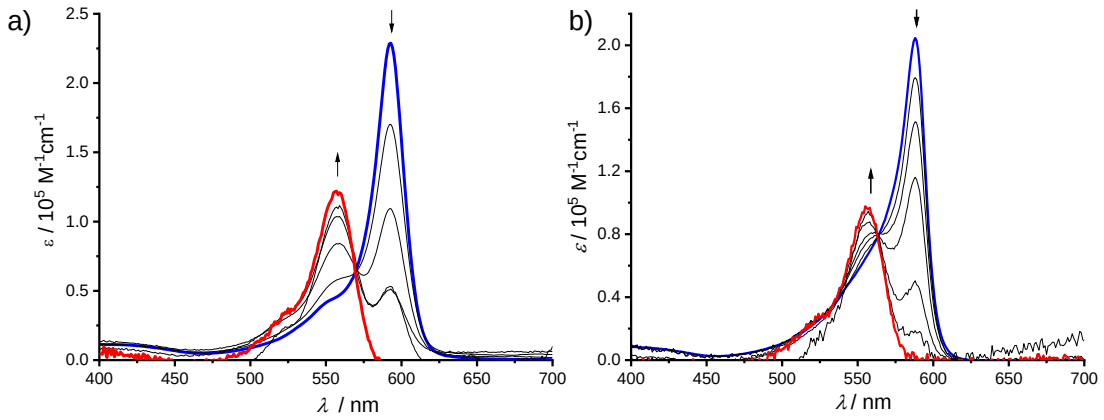

Fig. S21. (a) UV/Vis absorption spectra of BODIPY dye **1b** in different concentrations of *n*-hexane solution (2.0×10^{-6} M to 1.0×10^{-7} M) at 40°C; (b) UV/Vis absorption spectra of BODIPY dye **1c** in different concentrations of *n*-hexane solution (1.0×10^{-5} M to 1.0×10^{-7} M) at 25°C.

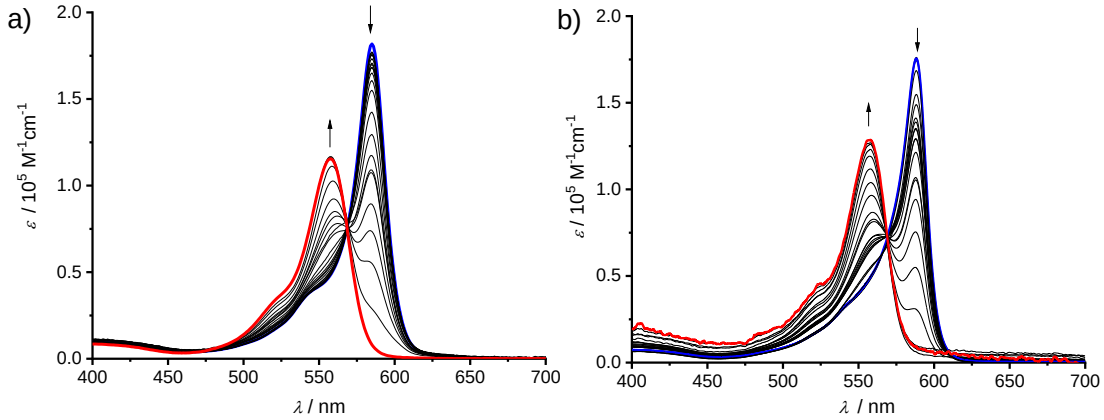

Fig. S22. (a) UV/Vis absorption spectra of BODIPY dye **1b** in different concentrations of MCH solution (8.0×10^{-5} M to 9.0×10^{-7} M) at 25°C; (b) UV/Vis absorption spectra of BODIPY dye **1c** in different concentrations of MCH solution (8.0×10^{-5} M to 1.0×10^{-5} M) at 25°C.

7. Concentration-dependent ^{1}H NMR spectroscopic studies

The concentration-dependent ^{1}H NMR data was fitted using the model developed by LaPlanche et al.[5] to derive the association constants for hydrogen bonding. The model describes the hydrogen bonding-directed assembly via an initial dimerization (Eq. 7) and higher order aggregation (Eq. 8).

$$2X \overset{K_2}{\rightleftharpoons} X_2 \tag{7}$$

$$X_{n-1} + X \overset{K}{\rightleftharpoons} X_n,\ n>2 \tag{8}$$

In the above expressions, X represents monomer and X_n represents the aggregated species composed of *n* monomers. In brief, the assumptions for simplifying the model are (1) the monomer-dimer equilibrium has a unique binding constant K_2; (2) the association constants *K* for higher order aggregation events are all equal; (3) the chemical shift of a proton in assembly X_n does not depend on *n* when $n \geq 2$; (4) the amount of hydrogen bonding between dye molecules and the solvent is negligible.

From the equations derived by LaPlanche, the chemical shift δ_{calcd} for a given proton in the above system satisfies

$$\delta_{calcd} = (\delta_1 - \delta_n)\alpha + \delta_n \tag{9}$$

$$\alpha = \left[\frac{\sigma^{n-1}(K[X])^n \frac{1}{1-K[X]} + K[X]}{\sigma^{n-1}(K[X])^n \left[\frac{n+(1-n)K[X]}{(1-K[X])^2}\right]}\right] \tag{10}$$

δ_1 is the chemical shift of the proton in the monomer.

δ_n is the chemical shift in aggregate species.

σ is cooperativity factor defined as K_2 / *K*.

[X] is the molar concentration of non-hydrogen bonded monomers, which can be solved from equation 11:

$$Kc_T = K[X] + \sum_{n=2}^{\infty} n \cdot K[X_n]$$

$$= K[X] + \sigma(K[X])^2 \frac{2-K[X]}{(1-K[X])^2}$$

$$= K[X] + \frac{2\sigma(K[X])^2 - \sigma(K[X])^3}{(1-K[X])^2} \tag{11}$$

where $[X_n]$ is defined as the concentration of the aggregate species. As equation 14 has only one real root subject to the physical constraints of the experiment, a [X] value for a given pair of K_2 and *K* can be determined explicitly for any experimental concentration.

Subsequently, the δ_{calcd} can be plotted as a function of Kc_T by substituting equation 10 and 11 into equation 9. Then the calculated δ_{calcd} - Kc_T curve can be manually fitted with the plot of δ_{obsd} versus Kc_T to find the best overall agreement between calculated curve and experimental data. Then values of K_2 and *K* can be determined.

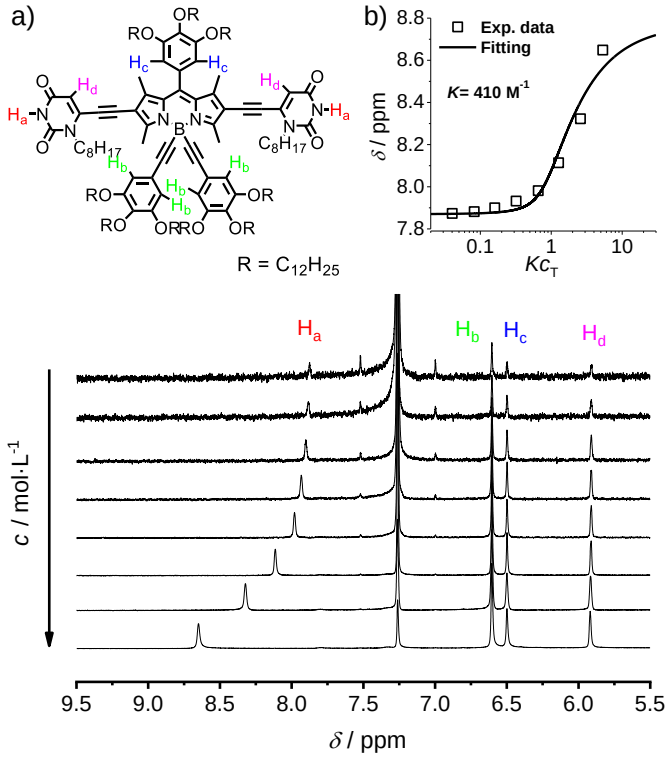

Fig. S23 Concentration-dependent ^{1}H NMR spectra of dye **1b** ($CDCl_3$, 400 MHz, 298 K). The arrow indicates the spectroscopic changes with increasing concentration from 9.8 × 10^{-5} M to 1.3 × 10^{-2} M. Inset: The structure of dye **1b** and plot of chemical shift of H_a in dye **1b** versus dimensionless concentration Kc_T and the fitting curve calculated with LaPlanche model.

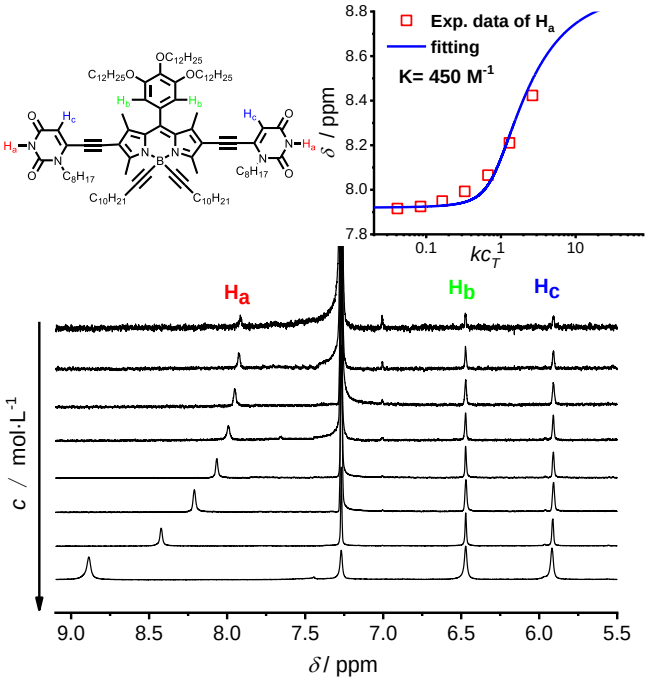

Fig. S24 Concentration-dependent ^{1}H NMR spectra of dye **1c** ($CDCl_3$, 400 MHz, 298 K). The arrow indicates the spectroscopic changes with increasing concentration from 9.8 × 10^{-5} M to 1.3 × 10^{-2} M. Inset: The structure of dye **1c** and plot of chemical shift of H_a in dye **1c** versus dimensionless concentration Kc_T and the fitting curve calculated with LaPlanche model.

8. Studies based on molecular exciton theory

The theoretical absorption spectral shift arising from the "brickwork" arrangement of BODIPY chromophores can be estimated by Kasha's molecular exciton model,[6] which is based on the point-dipole approximation and the assumption of additive increments for each pairwise interaction between dye neighbors in extended aggregates. The spectral shift is determined by the distance between two interacting dye neighbors as well as the angle between the aggregation direction and the connecting line of two point dipoles. At short distances and small angles (< 54.7 °) between the molecules, the UV/Vis absorption spectrum could be significantly red-shifted.

The equation 12 can be used to calculate the splitting of excited state energy levels caused by exciton coupling between aggregated molecules.

$$\varepsilon = \frac{|\mu_{eg}|^2}{4\pi\varepsilon_0 r_{uv}^3}(1 - 3cos^2\theta) \tag{12}$$

where μ_{eg} is the transition dipole moment of the monomer, ε_0 the permittivity of vacuum, r_{uv} the distance between centers of adjacent molecules u and v, and θ is the slip angle that results from the translational offset of these two parallel-arranged molecules. The transition dipole moment of the monomer can be obtained by equation 13.

$$|\mu_{eg}|^2 = \frac{3hc\varepsilon_0 ln10}{2\pi^2 N_A} \cdot \int_{\tilde{\nu}_1}^{\tilde{\nu}_2} \frac{\varepsilon(\tilde{\nu})}{\tilde{\nu}} d\tilde{\nu} \tag{13}$$

in which $\varepsilon(\tilde{\nu})$ is the molar extinction coefficient, c the speed of light (2.9979 × 10^{10} cm s^{-1}), h the Planck's constant (6.6262 × 10^{-34} Js), ε_0 the permittivity of vacuum (8.8542 × 10^{-12} $C^2J^{-1}m^{-1}$).

The calculated results of transition dipole moments for dyes **1a-c** are listed in paper. Substituting the transition dipole moment into equation 12 yields the value for the exciton splitting. Then equation 14 is used to calculate the spectral shift caused by exciton coupling between neighboring molecules

$$\Delta\tilde{\nu} = \frac{\varepsilon}{hc} \tag{14}$$

Assuming that the exciton coupling occurs between adjacent molecules in the direction of hydrogen bond and in the direction of π-π stacking, the experimental and theoretical values of spectral wavenumber movement should satisfy the following relation.

$$\Delta\tilde{\nu}_{ex} < 2\frac{\varepsilon_H}{hc} + 2\frac{\varepsilon_\pi}{hc} + 2\frac{\varepsilon_{\pi'}}{hc} \tag{15}$$

The employed geometrical parameters for calculation were obtained from the molecular modeling of the tetramers (Fig. 5 and Fig. S25). The parameters are illustrated in Fig. 5b, which include the distances between chromophore centers in hydrogen bonding direction (r_H) and π-π stacking direction (r_π, r_π'), the offset angles caused by the slipped arrangement between two hydrogen bonded molecules (ϑ_H) and two π-π stacked molecules (ϑ_π, ϑ_π') relative to the aggregation direction. As a result, the calculated spectral shifts for the J-aggregates of dyes **1a, b, c** are $\Delta\tilde{\upsilon}$ < -1371 cm^{-1}, $\Delta\tilde{\upsilon}$ < --895 cm^{-1}, $\Delta\tilde{\upsilon}$ < -957 cm^{-1} respectively, which are in agreement with the experimental values (Table 3).

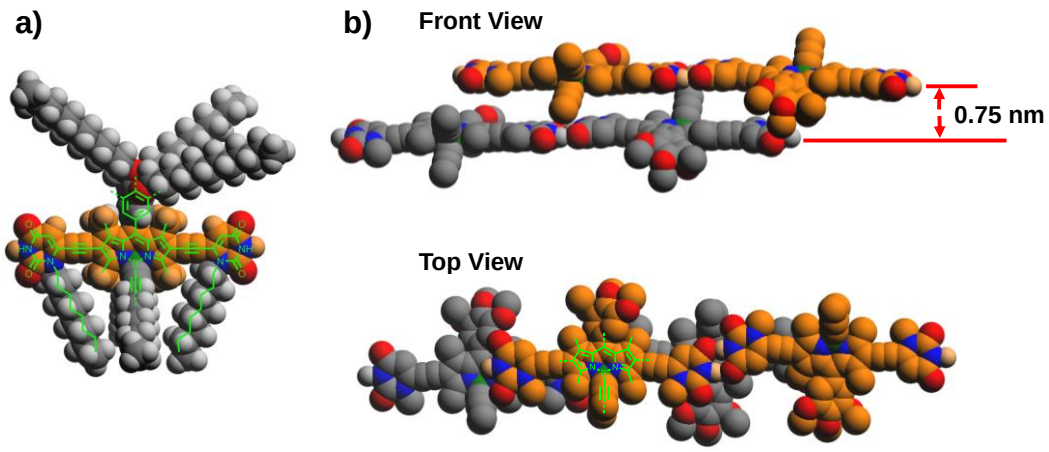

Fig. S25 (a) CPK model of BODIPY dye **1c** with geometry optimized on PM6 level in MOPAC program; (b) Geometrically optimized tetrameric aggregate of **1c** with PM6-D3H4 method (Alkyls and hydrogen atoms not involved in H-bonding are omitted for clarity in the figure).

9. References

1. G. Fan, Y. Lin, L. Yang, F. Gao, Y. Zhao, Z. Qiao, Q. Zhao, Y. Fan, Z. Chen and H. Wang, Co-self-assembled nanoaggregates of BODIPY amphiphiles for dual colour imaging of live cells, *Chem. Commun.*, 2015, **51**, 12447.
2. T. Moriuchi, S. Noguchi, Y. Sakamoto and T. Hirao, Synthesis and characterization of bioorganometallic conjugates composed of NCN-pincer platinum(II) complexes and uracil derivatives, *J. Organomet. Chem.*, 2011, **696**, 1089.
3. (a) P. Jonkheijm, P. van der Schoot, A. Schenning and E. W. Meijer, Probing the solvent-assisted nucleation pathway in chemical self-assembly, *Science*, 2006, **313**, 80; (b) M. M. J. Smulders, A. P. H. J. Schenning and E. W. Meijer, Insight into the mechanisms of cooperative self-assembly: The "sergeants-and-soldiers" principle of chiral and achiral C-3-symmetrical discotic triamides, *J. Am. Chem. Soc.*, 2008, **130**, 606.
4. (a) R. F. Goldstein and L. Stryer, Cooperative polymerization reactions. Analytical approximations, numerical examples, and experimental strategy, *Biophys. J.*, 1986, **50**, 583. (b) G. Fernández, M. Stolte, V. Stepanenko, and F. Würthner, Cooperative Supramolecular Polymerization: Comparison of Different Models Applied on the Self-Assembly of Bis(merocyanine) Dyes, *Chem. Eur. J.* 2013, **19**, 206-217.
5. (a) L. A. LaPlanche, H. B. Thompson and M. T. Rogers, Chain AssociationEquilibria. A Nuclear Magnetic Resonance Study of the Hydrogen Bonding of N-Monosubstituted Amides, *J. Phys. Chem.*, 1964, **69**, 1482; (b) W. S. Horne, C. D. Stout and M. R. Ghadiri, A heterocyclic peptide nanotube, *J. Am. Chem. Soc.*, 2003, **125**, 9372.
6. T. E. Kaiser, V. Stepanenko and F. Würthner, Fluorescent J-Aggregates of Core-Substituted Perylene Bisimides: Studies on Structure-Property Relationship, Nucleation-Elongation Mechanism, and Sergeants-and-Soldiers Principle, *J. Am. Chem. Soc.*, 2009, **131**, 6719.